Transformation of Surface Waves in Homogeneous Absorbing Layers

Pyotr Y. Ufimtsev, *Fellow, IEEE*, R. T. Ling, and J. D. Scholler, *Member, IEEE*

***Abstract*—Surface waves in homogeneous absorbing layers are studied. The transformation of surface waves into other types of guided waves with frequency or layer's parameters variations is analyzed. It is found that in absorbing layers the standing damped surface waves do not exist and *continuous transformation* of surface waves into leaky waves is forbidden. Surface waves can only transform continuously into nonphysical waves with field strengths increasing exponentially in both the direction of propagation and in normal direction away from the layer into free-space. The frequency at which surface waves transform into nonphysical waves can be considered as cutoff frequency of surface waves. New and more general definitions previously proposed by the authors for the phase and energy velocities of guided waves are analyzed. It is shown that these velocities are identically equal to each other and never exceed the light speed in free-space. Several new physical phenomena are discovered. These are the upper frequency cutoff, its shifting to higher frequencies for materials with lower losses and the merging of high TE wave modes.**

***Index Terms*—Absorbing media, electromagnetic surface waves.**

I. Introduction

SURFACE wave in homogeneous lossless layers is a classical subject of the guided waves theory. Properties of surface waves in absorbing layers are not well known. Only recently have they been studied in details by the present authors [1]–[7]. In particular, it was found that in absorbing layers, TM surface waves cannot propagate if the frequency exceeds the so-called upper cutoff frequency. At this upper cutoff frequency a TM surface wave becomes a regular plane wave incident on an absorbing layer at the Brewster angle. In this connection, we recall that, in general, surface waves can be interpreted as inhomogeneous plane waves incident on a flat guiding surface under the complex Brewster angle without reflection [6], [8], [9]. The complex Brewster angle is defined by of [6, eqs. (26)–(28)]. Note also that in (42) of [6], an additional factor of 1/2 was overlooked. Therefore, all expressions and numerical data for the energy velocity presented in [6], except the definition (40), must be multiplied by a factor of two. These corrections are published in [7].

In the present paper, we continue the study of surface waves. New and more general definitions for the phase and energy velocities, which were introduced in [6], [7], are analyzed in Section II. It is shown that these velocities are always identically equal to each other. Some general properties of guided waves in the complex plane of the transverse wave number are considered in Section III. They include the rotation of the Poynting vector and all possible values of the phase and energy velocities of guided waves. It is found that these velocities never exceed the light velocity. Absence of standing damped surface waves in absorbing layers is demonstrated in Section IV. Continuous transformation of guided waves in absorbing layers is studied in Section V. It is found that a *continuous transformation* of surface waves into leaky waves is forbidden. Several new physical phenomena are discovered. These are the upper frequency cutoff, its shift to higher frequencies in materials with lower losses and the merging of fundamental and higher order TE modes. These phenomena are described in Sections VI–VIII.

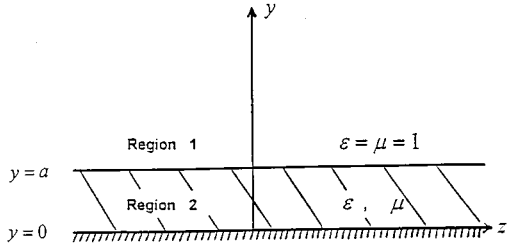

Fig. 1. Absorbing layer $(0 \le y \le a)$ backed up by a perfectly conducting plane $(y = 0)$.

II. Basic Characteristics of Surface Waves

We consider surface waves in a homogeneous absorbing layer placed on a perfectly conducting plane (Fig. 1). The thickness of the layer is denoted by the letter a, its relative permittivity and permeability are ϵ and μ, respectively. A free-space $(\varepsilon = \mu = 1)$ is assumed to be above the layer. The wave number in free-space is denoted as $k_0 = \omega\sqrt{\varepsilon_0\mu_0} = 2\pi/\lambda_0$ where ω is the angular frequency of harmonic oscillations and λ_0 is the free-space wavelength. The time dependence $\exp(-i\omega t)$ is assumed and suppressed below. We consider both TM and TE surface waves. The TM waves are described by equations

$$H_x = e^{ik_1(y-a)}e^{i\beta z},$$
$$E_y = -\frac{\beta}{k_0}Z_0H_x, \quad E_z = \frac{k_1}{k_0}Z_0H_x \tag{1}$$

in the free-space (Region 1), $y \ge a$ and by equations

$$H_x = \frac{\cos(k_2y)}{\cos(k_2a)}e^{i\beta z},$$
$$E_y = -\frac{\beta}{k_0\varepsilon}Z_0H_x, \quad E_z = i\frac{k_2}{k_0\varepsilon}Z_0H_x\tan(k_2y) \tag{2}$$

Manuscript received July 27, 1998; revised July 28, 1999.

P. Y. Ufimtsev is with the Northrop Grumman Corporation, Pico Rivera, CA 90660-3783 USA. He is also with the Electrical Engineering Department, University of California at Los Angeles, Los Angeles, CA 90095-1594 USA.

R. T. Ling was with the Northrop Grumman Corporation, Pico Rivera, CA 90660-3783 USA. He is now with the Technical University at Hamburg, Germany.

J. D. Scholler is with the Northrop Grumman Corporation, Pico Rivera, CA 90660-3783 USA.

Publisher Item Identifier S 0018-926X(00)01647-1.

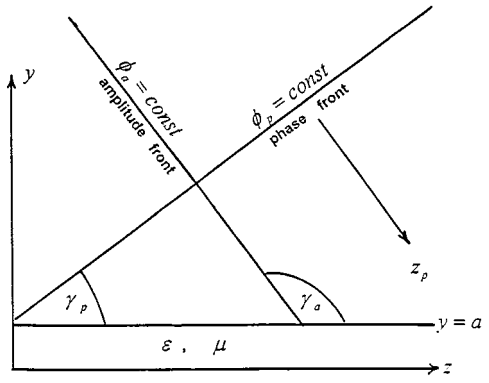

Fig. 2. Amplitude and phase fronts of the surface wave above the layer.

inside the layer (Region 2), $0 \le y \le a$. In these equations, $Z_0 = \sqrt{\mu_0/\varepsilon_0}$ is the impedance of the free-space. The complex quantities $k_1 = k_1' + ik_1''$ and $k_2 = k_2' + ik_2''$ are the transverse wave numbers of the wave field outside and inside the layer, respectively. The complex quantity $\beta = \beta' + i\beta''$ is the longitudinal wave number, or the propagation constant. These wave numbers are connected by the relations

$$k_1^2 + \beta^2 = k_0^2, \quad k_2^2 + \beta^2 = k_0^2\varepsilon\mu \tag{3}$$

through the Helmholtz wave equation. It follows that

$$k_2^2 - k_1^2 = k_0^2(\varepsilon\mu - 1). \tag{4}$$

The H_x components from (1) and (2) are continuous on top of the layer ($y = a$). The E_z-component satisfies the boundary condition on the perfectly conducting plane ($E_z = 0$ at $y = 0$) and its continuity on top of the layer $y = a$ leads to a transcendental relationship

$$k_1\varepsilon = ik_2 \tan(k_2 a). \tag{5}$$

This transforms into the dispersion equation

$$D^{TM}(k_0,\beta) \equiv \sqrt{k_0^2\varepsilon\mu - \beta^2}\tan(a\sqrt{k_0^2\varepsilon\mu - \beta^2}) + i\varepsilon\sqrt{k_0^2 - \beta^2} = 0 \tag{6}$$

with the substitutions of k_1 and k_2 from (3).

The time-averaged Poynting vector $\vec{P} = \frac{1}{2}\ \mathrm{Re}[\vec{E} \times \vec{H}^*]$ points in the direction of the power flux. Above the layer it contains the components

$$P_y = \frac{k_1'}{2\omega\varepsilon_0} e^{-2[k_1''(y-a)+\beta'' z]}$$
$$P_z = \frac{\beta'}{2\omega\varepsilon_0} e^{-2[k_1''(y-a)+\beta'' z]}. \tag{7}$$

Their ratio equals

$$P_z/(-P_y) = -\frac{\beta'}{k_1'} = \tan\gamma_p \tag{8}$$

where γ_p is the angle between the phase front and the z-axis (Fig. 2). The Poynting vector of surface waves is perpendicular to the phase front and directed along the amplitude front. The angle γ_a in Fig. 2 determines the orientation of the amplitude front. This angle is given by

$$\tan\gamma_a = -\frac{\beta''}{k_1''}. \tag{9}$$

According to the first equality in (3),

$$\tan\gamma_a = -\frac{\beta''}{k_1''} = \frac{k_1'}{\beta'} = -\cot\gamma_p. \tag{10}$$

The TE surface waves are described by similar equations. Their field components above the layer ($y \ge a$) are

$$E_x = e^{ik_1(y-a)}e^{i\beta z}$$
$$H_y = \frac{\beta}{k_0}Y_0 E_x, \qquad H_z = -\frac{k_1}{k_0}Y_0 E_x \tag{11}$$

and inside the layer ($0 \le y \le a$) they are

$$E_x = \frac{\sin(k_2 y)}{\sin(k_2 a)}e^{i\beta z}$$
$$H_y = \frac{\beta}{k_0\mu}Y_0 E_x, \qquad H_z = i\frac{k_2}{k_0\mu}Y_0 E_x\cot(k_2 y) \tag{12}$$

where $Y_0 = 1/Z_0$ is the admittance of free-space.

The wave numbers k_1, k_2, β of TE waves also obey (3) and (4). But instead of (5) for TM waves, they satisfy the dispersion equation

$$k_1\mu = -ik_2\cot(k_2 a) \tag{13}$$

which can be written as

$$D^{TE}(k_0,\beta) \equiv \sqrt{k_0^2\varepsilon\mu - \beta^2}\cot(a\sqrt{k_0^2\varepsilon\mu - \beta^2}) - i\mu\sqrt{k_0^2 - \beta^2} = 0. \tag{14}$$

Above the layer, the time-averaged Poynting vector of TE waves contains the components

$$P_y = \frac{k_1'}{2\omega\mu_0} e^{-2[k_1''(y-a)+\beta'' z]}$$
$$P_z = \frac{\beta'}{2\omega\mu_0} e^{-2[k_1''(y-a)+\beta'' z]}. \tag{15}$$

Their ratio is given by (8) where the quantities k_1 and β satisfy (14). Thus, in the case of TE waves, the Poynting vector is also perpendicular to the phase front.

In [6], [7] we introduced new definitions for the phase velocity $\vec{v}_p$ and the energy velocity $\vec{v}_e$ of TM and TE surface waves above the layer . These velocities are perpendicular to the phase front and directed toward the absorbing layer (Fig. 2). The phase velocity is the speed of the phase front propagation. The energy velocity is defined as the ratio $\vec{v}_e = \vec{P}/w$, where $\vec{P}$ is the power flux density (the Poynting vector) and w is the volume energy density. According to [6], [7], the quantities $\vec{v}_p$ and $\vec{v}_e$ are determined by the following expressions:

$$\frac{\vec{v}_p}{c} = \frac{k_0}{\sqrt{\beta'^2 + k_1'^2}}\hat{z}_p$$
$$\frac{\vec{v}_e}{c} = 2\frac{k_0\sqrt{k_1'^2 + \beta'^2}}{k_0^2 + |k_1|^2 + |\beta|^2}\hat{z}_p. \tag{16}$$

Using the dispersion relation $k_1^2 + \beta^2 = k_0^2$, one can show that the energy velocitiy is identically equal to the phase velocity

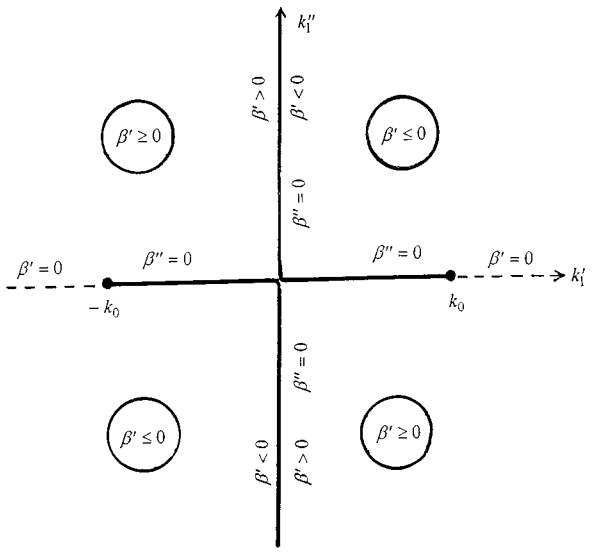

Fig. 3. The first Riemann sheet $[\mathrm{Im}(\beta) \geq 0]$.

$(\vec{v}_e \equiv \vec{v}_p)$. It is necessary to emphasize the distinction in principle between our definition for the phase velocity and the conventional definition for the phase velocity $(\vec{v}^{con}/c = \hat{z} \cdot k_0/\beta')$, which is accepted in the theory of transmission lines. According to our definition (16), the phase velocity $\vec{v}_p$ is oriented under the oblique angle γ_a towards the layer surface in the direction $\hat{z}_p$, while the conventional phase velocity $\vec{v}_p^{con}$ is oriented parallel with the layer surface in the direction $\hat{z}$ (Fig. 2). In the particular case of lossless structures $(\beta'' = 0, k_1' = 0, \hat{z}_p = \hat{z})$, the quantity $\vec{v}_p$ determined by (16) exactly coincides with $\vec{v}_p^{con}$. Therefore, our definition for the phase velocity (16) can be considered as a natural generalization of the conventional phase velocity for the case of absorbing guiding structures. Note also that our definition for the energy velocity $\vec{v}_e$ is completely different from the conventional group velocity $(\vec{v}_{group} = \hat{z} \cdot \partial\omega/\partial\beta')$, which is not applicable in the case of absorbing and dispersive guiding structures. This is clearly shown in Fig. 23 of [6].

III. Diagrams of Guided Waves

The complex plane of the transverse free-space wave number $k_1 = k_1' + ik_1''$ is often used in the analysis of guided waves [10]–[13]. The longitudinal wave number $\beta = \sqrt{k_0^2 - k_1^2}$ is a single-valued function in the two-sheet Riemann k_1-plane with two branch cuts shown in Fig. 3. The upper branch cut starts at $k_1 = k_0$ on the positive real axis, moves towards the origin and turns upwards along the positive imaginary axis. The lower branch cut starts at $k_1 = -k_0$ on the negative real axis, moves towards the origin and turns downwards along the negative imaginary axis. On these cuts, the imaginary part of the longitudinal wave number equals zero $\mathrm{Im}(\beta) \equiv \beta'' = 0$. We assume Im $(\beta) \geq 0$ on the first Riemann sheet and Im $(\beta) \leq 0$ on the second sheet. Note also that on the first Riemann sheet, the real part of longitudinal wave number is negative $(\beta' < 0)$ in the first and third quadrants and positive $(\beta' > 0)$ in the second and fourth quadrants (Fig. 3). On the second Riemann sheet, $\beta' > 0$ in the first and third quadrants and $\beta' < 0$ in the second and fourth quadrants.

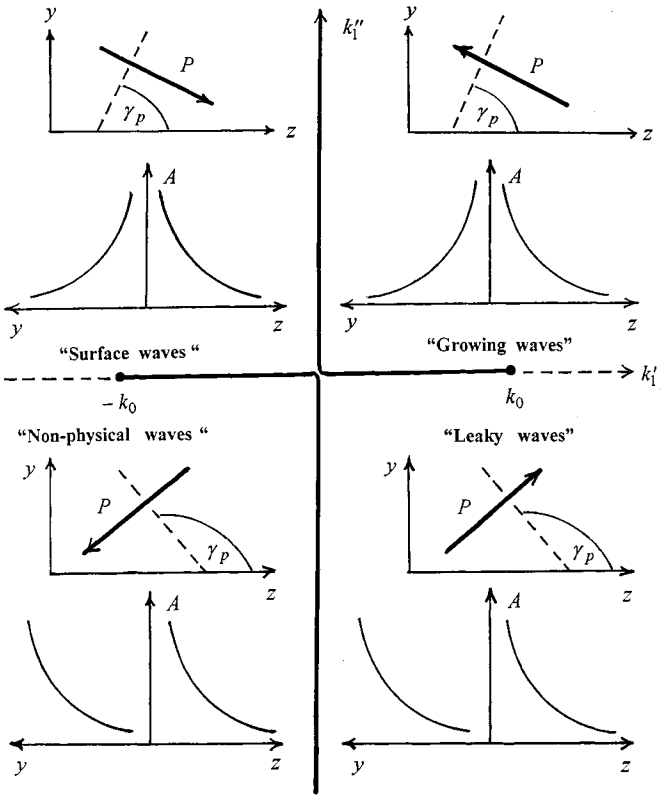

Fig. 4. The diagram of guided waves in the first Riemann sheet $[\mathrm{Im}(\beta) \geq 0]$.

There is a common functional form for all possible guided waves in each Riemman sheet. All of these waves can be written in the form $\exp\{i[k_1'(y-a)+\beta' z] - k_1''(y-a) - \beta'' z\}$. Since the parameters k_1', k_1'' and β' have different sign combinations in various quadrants of the Riemann sheets, the guided waves in different quadrants have different physical properties. However, outside the open guiding structures, all of them are inhomogeneous plane waves.

Figs. 4 and 5 show the wave diagrams for the first and second Riemann sheets. These diagrams explain the qualitative behavior of the wave amplitude $A(y,z) = \exp[-k_1''(y-a) - \beta'' z]$ as a function of the distance y from the layer and the distance z along the layer. They also show the directions of the Poynting vector, which is always perpendicular to the phase fronts.

We adopt the following terminology for guided waves in these diagrams. "*Growing waves*," shown in the first quadrant, *increase* exponentially in the direction of propagation along the layer and *decrease* exponentially in the direction away from the layer. They can be excited in amplifying systems. In passive lossless systems these waves always exist in pairs with guided waves from the second quadrant and combine into standing damped waves [10]–[12]. We consider these waves in more details below. "*Surface waves*," shown in the second quadrant, *decrease* exponentially both in the direction away from the layer and in the direction of propagation along the layer. "*Nonphysical waves*" in the third quadrant *increase* exponentially both in the direction of propagation along the layer and in the direction away from the layer. "*Leaky waves*" in the fourth quadrant *increase* exponentially in the direction

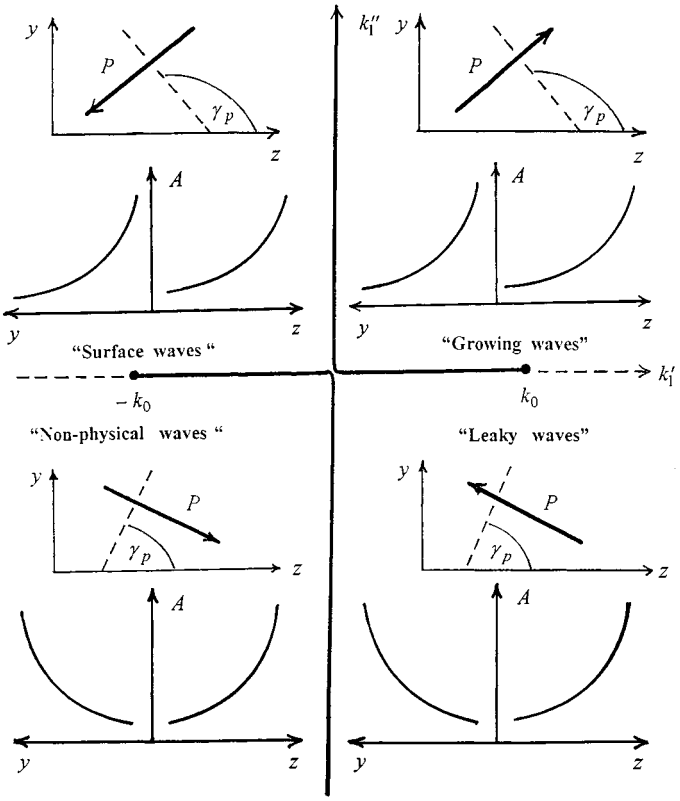

Fig. 5. The diagram of guided waves in the second Riemann sheet $[\mathrm{Im}(\beta) \leq 0]$.

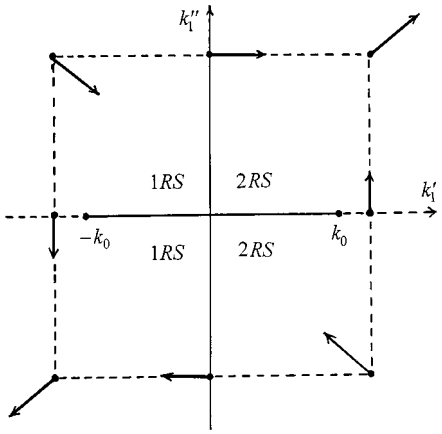

Fig. 6. Rotation of the Poynting vector on the contour, which intersects branch cuts two times.

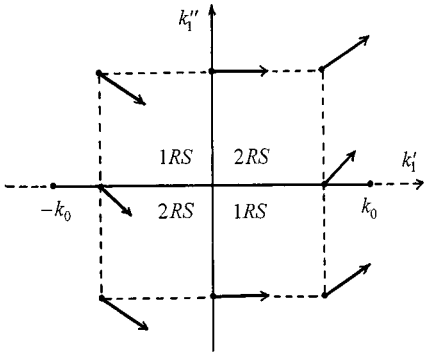

Fig. 7. Rotation of the Poynting vector on the contour, which intersects branch cuts four times.

away from the layer and *decrease* exponentially in the direction of propagation along the layer. The term "leaky" implies that these waves transfer energy out of the guiding structure. All these types of guided waves can be considered as analytical continuations of surface waves in the complex plane (k_1', k''_1).

Note that the complex β-plane also can be used for analysis of guided waves. However, it is less convenient than the complex k_1-plane because each Riemann sheet of the β-plane contains only two types of guided waves. Its first sheet $(\mathrm{Im}(k_1) > 0)$ contains only the surface and growing waves, while the second sheet $(\mathrm{Im}(k_1) < 0)$ contains only the nonphysical and leaky waves. In contrast to this, each Riemann sheet of the complex k_1-plane contains all four types of guided waves.

Some interesting features of guided waves can be seen from the these diagrams shown in Figs. 4 and 5. Let us consider closed contours in the complex plane (k_1', k''_1) that intersect the branch cuts. Symbols 1RS and 2RS denote the respective quadrant in complex plane belonging to the first or second Riemman sheet. Figs. 6 and 7 show the orientations of Poynting vector along closed contours indicated by broken lines. These contours in general can have arbitrary shapes. For simplicity, we have chosen the square contours. In these figures we assume that Poynting vector is expressed in Cartesian coordinates y and z oriented along axes k''_1 and k_1', respectively, as defined in Figs. 4 and 5. The contour in Fig. 6 intersects the branch cuts twice. As the point (k_1', k''_1) moves along the contour, the Poynting vector undergoes a rotation. The sense of this rotation is opposite to the sense in which the point (k_1', k''_1) moves along the contour. When this point moves clockwise along the contour, the Poynting vector rotates counter-clockwise and vice versa. The closed contour indicated by the broken lines in Fig. 7 intersects the branch cuts four times. When the point (k_1', k''_1) moves from the left half-plane $(k_1' \leq 0)$ into the right half-plane $(k_1' \geq 0)$ along the horizontal lines, the Poynting vector rotates counter-clockwise. The sense of the Poynting vector rotation is not constant on the vertical lines of the contour. For example, along the left vertical line in Fig. 7, the Poynting vector rotates clockwise before the point (k_1', k''_1) in the second quadrant moves down and intersects the real axis. In the third quadrant, the Poynting vector rotates counter-clockwise after the point (k_1', k''_1) crosses the real axis and moves down. However, the total angle of rotation in each direction does not exceed 45°. We do not consider here the behavior of the Poynting vector on closed contours which do not cross the branch cuts since it is clearly shown in Figs. 4 and 5.

According to (16), moduli of the phase and energy velocities are functions symmetrical with respect to the k_1'- and k''_1-axes. Numerical calculations show that these velocities do not exceed the light velocity anywhere $(v_{p,e} \leq c)$. They are close to the light velocity near the origin in the k_1-plane and then decrease as the point (k_1', k''_1) moves away. At a distance $\rho = \sqrt{(k'/k_0)^2 + (k''/k_0)^2} \approx 10^2$ from the origin, the moduli of the phase and energy velocities approach values of the order $c \cdot 10^{-2}$. Using the dispersion equation $k_1^2 + \beta^2 = k_0^2$, one can show that $\sqrt{\beta'^2 + k_1'^2} > k_0$. Therefore, according to (16), we

have $\vec{v}_{e,p} \leq c$. This means that all guided waves presented in diagrams in Figs. 4 and 5 are slow waves.

It is to be noted that diagrams in Figs. 4 and 5 relate to any guiding structures homogeneous in the planes $y = \text{const}$ (Fig. 1). However, their constitutive parameters ϵ and μ can depend arbitrarily on the coordinate y. In particular, such guiding structures can consist of arbitrarily stratified material.

IV. Absence of Standing Damped Guided Waves in Homogeneous Absorbing Layers

As it is well known [10]–[12] for lossless structures, the growing guided waves from the first quadrant on the wave diagrams (Figs. 4 and 5) always exist in pairs with surface guided waves from the second quadrant. These pairs form standing damped waves excited in the vicinity of a field source. As it is mentioned in [10]–[12], this type of waves does not exist in lossy structures. This is proven below for any homogeneous absorbing layers. In the region to the right of the source $(z > z_{source})$, the standing wave can be represented as the sum

$$u = u^{sw} \pm u^{gw}. \tag{17}$$

Here

$$u^{sw} = \exp[i(k_1^{sw} y + \beta^{sw} z)] \tag{18}$$

is the surface wave with the wave numbers (k_1^{sw}, β^{sw}) from the second quadrant in the first Riemman sheet (Fig. 4) and

$$u^{gw} = \exp[i(k_1^{gw} y + \beta^{gw} z)] \tag{19}$$

is the growing wave with the wave numbers (k_1^{gw}, β^{gw}) from the first quadrant in the same Riemman sheet. These two waves u^{sw} and u^{gw} can form a standing damped wave only in the case when their wave numbers satisfy the following relationships:

$$k_1^{gw} = -(k_1^{sw})^*, \quad \beta^{gw} = -(\beta^{sw})^* \tag{20}$$

where the symbol $(\cdots)^*$ denotes the complex conjugate. In addition, the wave numbers related to the region inside the layer must satisfy the equation

$$k_2^{gw} = \pm k_2^{sw}. \tag{21}$$

All these wave numbers must also satisfy the dispersion equations (3)–(6), (13), and (14). Let us check the validity of (3) for wave numbers k_1^{gw}, k_2^{gw} and β^{gw}. Starting with the equation for the wave numbers k_1^{gw} and β^{gw}, we have

$$\begin{aligned}(k_1^{gw})^2 + (\beta^{gw})^2 &= [(k_1^{sw})^*]^2 + [(\beta^{sw})^*]^2 \\ &= [(k_1^{sw})^2]^* + [(\beta^{sw})^2]^* = k_0^2.\end{aligned} \tag{22}$$

Thus, the wave numbers k_1^{gw} and β^{gw} satisfy the first dispersion relation in (3).

Let us next check the validity of the second dispersion relation in (3)

$$\begin{aligned}(k_2^{gw})^2 + (\beta^{gw})^2 &= (k_2^{sw})^2 + [(\beta^{sw})^*]^2 \\ &= (k_2^{sw})^2 + [(\beta^{sw})^2]^* = (k_2^{sw})^2 + (\beta^{sw})^2 \\ &\quad + [(\beta^{sw})^2]^* - (\beta^{sw})^2 \\ &= k_0^2 \varepsilon\mu - 2i \operatorname{Im}[(\beta^{sw})^2] \neq k_0^2 \varepsilon\mu.\end{aligned} \tag{23}$$

Thus, the dispersion equation for the wave numbers inside *absorbing* layers [when $\operatorname{Im}(\beta^{sw}) > 0$] is violated. Therefore, standing damped waves cannot exist in homogeneous *absorbing* layers. It is clear also that such waves can exist only in those guiding structures where the dispersion equation $D(k_0, \beta) = 0$ remains valid when β is replaced by $(-\beta^*)$.

V. Continuous Transformations of Surface Waves in Absorbing Layers

On the complex plane of the transverse wave number, continuous transformation of surface waves means a movement of the point (k_1', k''_1) from the second quadrant into other quadrants (Fig. 8). A possibility of these transformations depends on the wave behavior at the transition points A, B, C, and D. At point A which lies on the upper branch cut, i.e., on the boundary between the first and second quadrants in the first Riemman sheet, the surface wave transforms into the wave $\exp(-k''_1 y + i\beta' z)$, which propagates along the layer without attenuation. This wave cannot exist in absorbing layers, therefore, the transformations of surface waves into growing waves is forbidden.

Next, let us consider the possible transformation of surface waves into leaky waves. Such a transformation implies the transition of the point (k_1', k''_1) from the second quadrant into the fourth quadrant through the point B where $k_1 = 0$ and $\beta = k_0$. At this point, the surface wave transforms into the plane wave $\exp(ik_0 z)$, which propagates along the layer without attenuation. Again in absorbing layers such a wave cannot exist. Therefore, in absorbing layers, the direct transformation of surface waves into leaky waves is forbidden.

It is of interest to note that the TM surface waves in lossless plasma layers can be continuously transformed, first into the growing waves and then into leaky waves when the wave frequency increases from zero to infinity. In particular, growing waves transform into leaky waves when the wave frequency exceeds the plasma frequency. This follows from in [10, fig. 16] and [11, fig. 3], if we use our classification of guided waves in Fig. 4 of the present paper. However, as shown above for absorbing layers, the continuous transition of the point (k_1', k''_1) from the second quadrant (with surface waves) into the first quadrant (with growing waves) is forbidden. Therefore, in absorbing layers this type of continuous transformation of surface waves into leaky weaves through the intermediate stage of growing waves is also forbidden.

Transformation of surface waves into nonphysical waves means the transition of the point (k_1', k''_1) from the second quadrant into the third quadrant (Fig. 8). This transition can occur through the point C or D. Point C lies on the lower branch cut while point D is beyond the branch cut. At the point C, the surface wave transforms into the regular plane wave $\exp[i(k_1' y + \beta' z)]$ incident on the layer under the Brewster angle without any reflection. At the point D, the surface wave transforms into an *inhonogeneous plane wave* $\exp(-i|k_1| y - \beta'' z)$. The amplitude of this wave exponentially decreases along the layer while the wave propagates in the direction normal to the layer. Since nonphysical waves cannot exist, the arrival of the point (k_1', k''_1) into the transition points C and D can be interpreted as a cutoff phenomenon. For

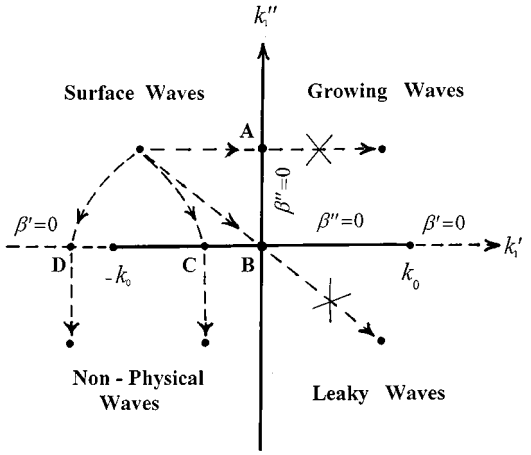

Fig. 8. Continuous transformation of surface waves.

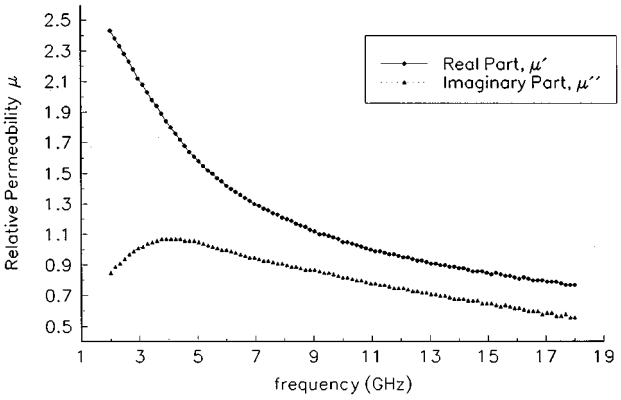

Fig. 9. Constitutive properties of sample material (constant relative permittivity: $\varepsilon' = 20.45, \varepsilon'' = 0.73$).

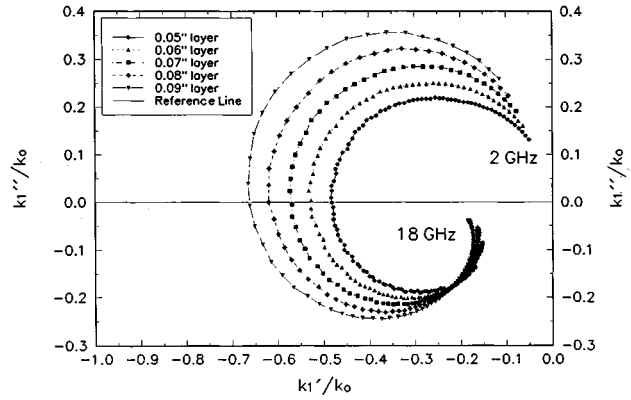

Fig. 10. Trajectories of the transverse wave number of fundamental TM guided waves in absorbing layers. The oscillation frequency ($f = c \cdot k_0/2\pi$) increases in the counter-clockwise direction along each trajectory.

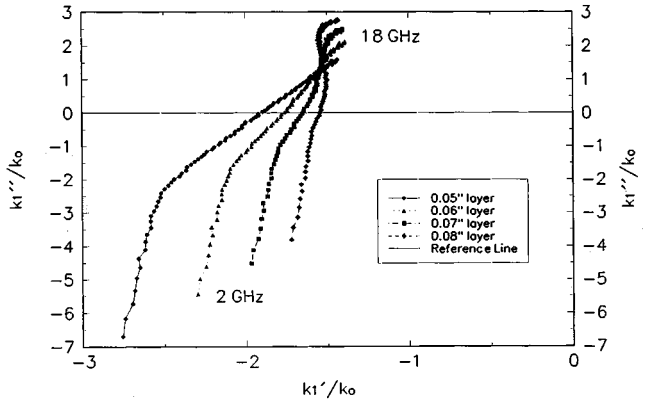

Fig. 11. Trajectories of the transverse wave number of fundamental TE guided waves in absorbing layers. The oscillation frequency ($f = c \cdot k_0/2\pi$) increases from the bottom to the top along each trajectory.

example, if the movement of the point (k_1', k''_1) is due to the frequency change, the frequency at the points C and D can be interpreted as a cutoff frequency of surface waves.

It is to be noted that the waves transformations described above and illustrated in Fig. 8 relate to any absorbing stratified guiding structures for both TM and TE types of guided waves. In the following, we present numerical data that illustrates the cutoff phenomenon in homogeneous layers. This data was obtained with the numerical solutions for dispersion equations (6) and (14) using the Muller's method [14]. All calculations were performed for an actual commercially available material with constitutive parameters shown in Fig. 9. Such materials are widely used as microwave absorbing coatings.

Transformation of TM surface waves into nonphysical waves through the point C (Fig. 8) is illustrated in Fig. 10 for absorbing layers with thickness a ranging from 0.05 to 0.09 inch. The oscillation frequency ($f = \omega/2\pi = ck_0/2\pi$) ranges from 2 GHz at the upper end of each trajectory in Fig. 10 to 18 GHz at its lower end. The frequency, at which the wave number trajectory crosses the real axis k_1' can be interpreted as the upper cutoff frequency. This phenomenon has been also described recently in [6]. As shown above, at this frequency the TM surface waves transform into regular plane wave incident on the absorbing layer under the real Brewster angle.

Fig. 11 illustrates the transformation of TE surface waves. In this figure, the point (k_1', k''_1) moves from the second quadrant into the third quadrant through the point D beyond the branch cut (Fig. 8) when the frequency decreases. Therefore, the frequency at which this point crosses the real axis k_1' can be interpreted as the usual lower cutoff frequency.

VI. An Upper Frequency Cutoff of TE Surface Waves

A new physical phenomenon, so far unknown, concerns an upper frequency cutoff for TE waves. It is shown in Figs. 12 and 13. The TE surface waves (with $k_1' < 0, k'' > 0, \beta' > 0$, and $\beta'' > 0$) shown in these figures can propagate only in finite frequency bands. The lower boundary of these bands is the usual lower cutoff frequency and the upper boundary is the upper cutoff frequency. In contrast to the case of TM surface waves, no specific values of the phase and energy velocities are inherent for upper cutoff frequencies.

Let us numerate the curves on Figs. 12 and 13 in the order of increasing frequency. It is obvious that all curves with numbers higher than one relate to high-order modes. The mode related to the first curve can be conditionally considered as fundamental. We cannot state that this is exactly a fundamental mode because

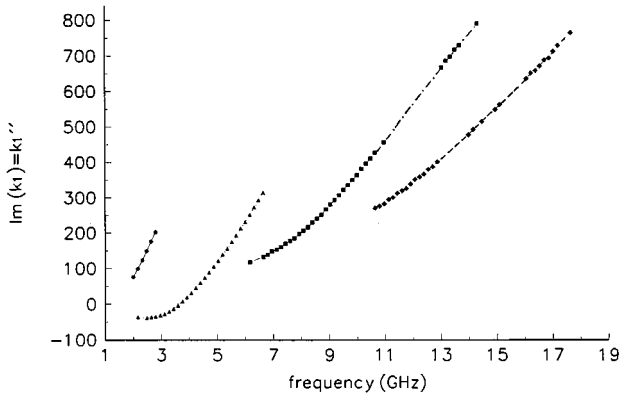

Fig. 12. Dispersion curves of TE surface waves in the absorbing layer with constitutive parameters shown in Fig. 9 and with thickness of 0.30 in. The transverse wave numbers of these waves are located in the second quadrant on the first Riemann sheet in the complex k_1-plane shown in Fig. 4

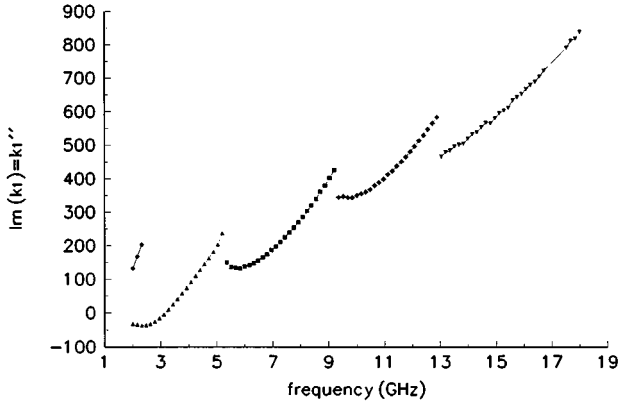

Fig. 13. Dispersion curves of TE surface waves in the absorbing layer with constitutive parameters equal to 1.2ε and 1.2μ, where ε and μ are shown in Fig. 9. The layer thickness equals 0.30 of inch. The transverse wave numbers of these waves are located in the second quadrant on the first Riemann sheet in the complex k_1-plane shown in Fig. 4.

we do not have the data for the constitutive parameters ε and μ at frequencies lower than 2 GHz. It may be that this mode also belongs to high-order modes.

Note also that the lower and upper cutoff phenomena for TE surface waves shown in Figs. 12 and 13 do not relate to the transition of their wavenumbers from the second quadrant into other quadrants or other Riemann sheets in the complex k_1-plane. Such transitions were not revealed in the numerical investigations of these waves. However, these transitions were obtained for surface waves in a thinner layer and they are shown below in Figs. 15 and 16.

The data in Fig. 12 relate to the actual absorbing layer with electromagnetic parameters given in Fig. 9. The data in Fig. 13 relate to the hypothetical absorbing layer which permittivity and permeability are 120% of original values given in Fig. 9. Note that the Kramers–Kronig relations are invariant with respect to a constant factor and allow multiplication of ε and μ by any constant real number. This property of the Kramers–Kronig relations is also used in the next section.

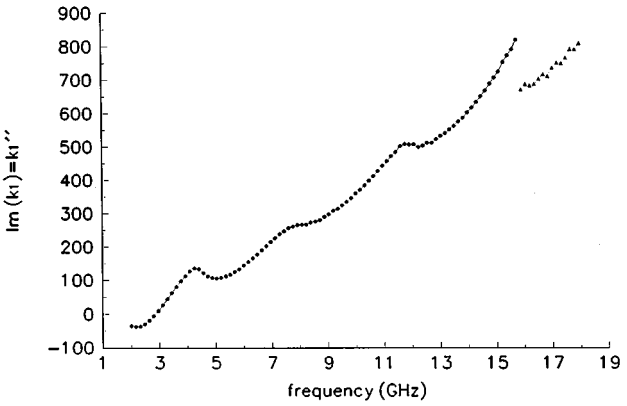

Fig. 14. Dispersion curves of TE surface waves in the absorbing layer with constitutive parameters equal to 1.35ε and 1.35μ where $\varepsilon$and μ are shown in Fig. 9. The layer thickness equals 0.30 of inch. The transverse wave numbers of these waves are located in the second quadrant on the first Riemann sheet in the complex k_1-plane shown in Fig. 4.

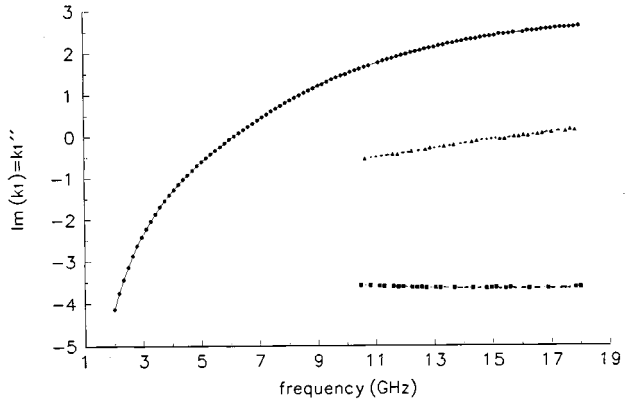

Fig. 15. Dispersion curves of TE wave modes in the absorbing layer with constitutive parameters shown in Fig. 9 . The layer thickness equals 0.075 of inch.

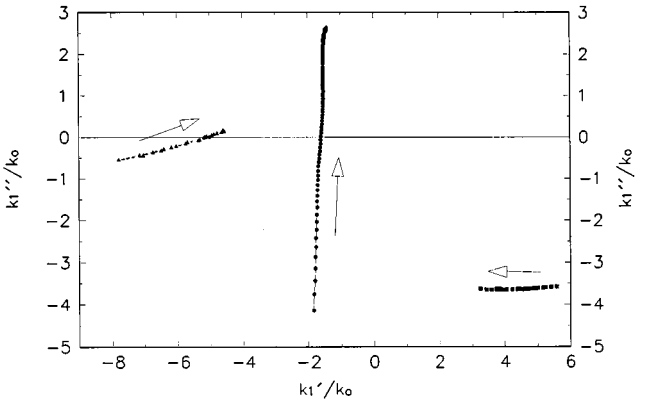

Fig. 16. Trajectories of the transverse wave number of those TE guided waves, which are shown in Fig. 15. The layer thickness equals 0.075 of inch. Constitutive parameters of the layer are given in Fig. 9. The directions at which the oscillation frequency ($f = c \cdot k_0/2\pi$) increases along each trajectory are shown by arrows.

VII. Merging of High TE Wave Modes

From observation of Figs. 12 and 13 it appears that the ends of neighboring trajectories tend to approach one another when

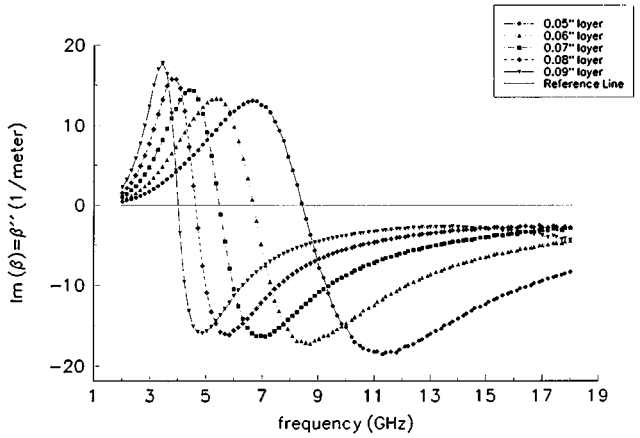

Fig. 17. Attenuation constants of TM surface waves in layers with constitutive parameters equal to 120% of original ε and μ, shown in Fig. 9.

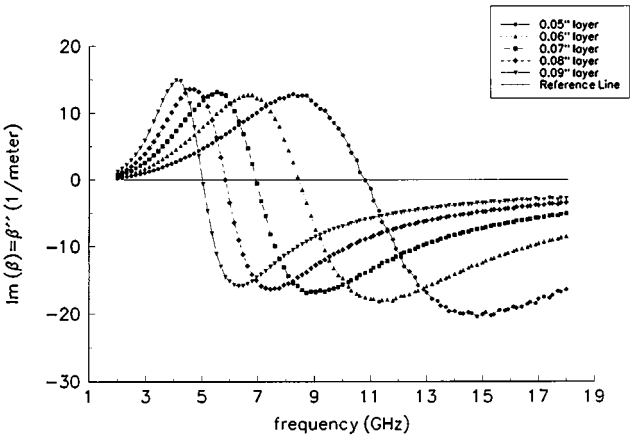

Fig. 18. Attenuation constants of TM surface waves in layers with original ε and μ, shown in Fig. 9.

ε and μ increase. In Fig. 14, it is seen that four trajectories of surface waves merge into one related to the fundamental mode (with $k_1' < 0, k'' > 0$, $\beta' > 0$, and $\beta'' > 0$) when the layer's permittivity and permeability reach 135% of original values given in Fig. 9. This is a newly discovered phenomenon. As with the upper frequency cutoff, it may have diverse practical applications. In particular, it can be used in the design of microwave devices with an extended single-mode frequency band.

VIII. Leaky Waves

Fig. 15 shows the dispersion characteristics of TE waves in a layer with 0.075 in thickness and with the original permittivity ε and permeability μ given in Fig. 9. The upper and middle curves represent the first (fundamental) and second modes, respectively. The lower curve relates to the leaky wave. This becomes clear from Fig. 16 where the dispersion characteristics of the same modes are displayed in the complex k_1-plane. The directions at which frequency f increases along dispersion trajectories are indicated by arrows. The left trajectory relates to the second mode. The central trajectory relates to the first (fundamental) mode. The frequencies at which these two trajectories intersect the real axis are the usual lower cutoff frequencies. The right trajectory in Fig. 16 is located in the fourth quadrant of the first Riemann sheet in Fig. 4 and represents a leaky wave. The left end of this trajectory represents the upper cutoff of the leaky wave.

Fig. 16 shows a continuous transformation of surface waves into nonphysical waves. However, changes of frequency and thickness of the layer with parameters ε and μ given in Fig. 9 do not reveal a continuous transformation of nonphysical waves into leaky waves. Other changes of thickness and ε, μ may reveal such a transformation.

IX. Shifting of the Upper Cutoff to Higher Frequencies in Materials with Lower Losses

Another interesting phenomenon is illustrated in Figs. 17–19, with dispersion curves for TM surface waves in lossy materials. In these figures, the positive values of the attenuation constant $\beta'' = \mathrm{Im}\ (\beta)$ relate to propagating surface waves while the negative values to nonphysical waves. Transformation of surface waves into nonphysical waves happens at the upper cutoff frequencies. Fig. 17 contains the dispersion curves for layers with the hypothetical material whose constitutive parameters are 120% of original ε and μ, shown in Fig. 9. In Fig. 18, we have the dispersion curves for layers with original ε and μ. In Fig. 19, the constitutive parameters are equal to 80% of original values. We recall again that multiplication of constitutive parameters by any positive constants does not violate the Kramers–Kronig relations. Comparison of these figures clearly shows that the upper cutoff frequencies increase when the absorbing layers become less lossy. The same observation follows from the comparison of the dispersion curves for TE surfaces waves in Figs. 12 and 13. This observation suggests the following idea: surface waves in all materials may have the upper frequency cutoff, but this cutoff happens at very high frequencies for materials with very low losses. This may explain why the upper cutoff phenomenon was not discovered in common materials with low losses which are used in transmission lines and microwave devices.

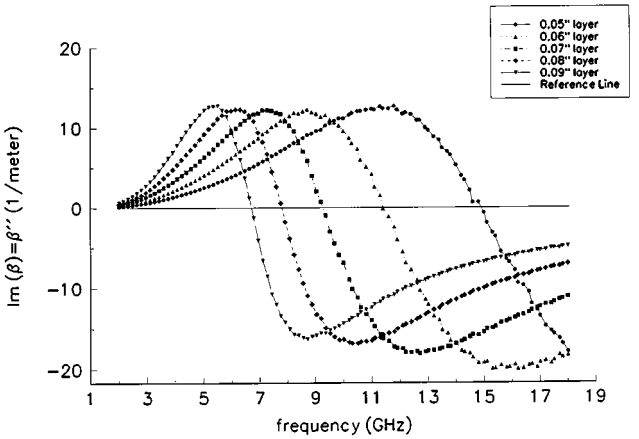

Fig. 19. Attenuation constants of TM surface waves in layers with constitutive parameters equal to 80% of original ε and μ, shown in Fig. 9.

X. Conclusion

Transformation of guided waves in absorbing layers has been investigated in the previous [6] and present papers. Characteristics of TM waves in such layers were studied in paper [6]. Gen-

eral properties of TM and TE guided waves in absorbing layers are the subjects of the present paper. It is shown that all waves guided by any homogeneous absorbing layers are slow waves. Their phase and energy velocities are identically equal to each other and always less than the light speed. It is also found that in such layers the continuous transformation of surface waves into growing and leaky waves is forbidden. New physical phenomena are discovered. These are the upper frequency cutoff for TM and TE surface waves, the shifting of the upper cutoff to higher frequencies in materials with lower losses, and the merging of high order TE wave modes.

The present paper supplements extensive publications on analytical investigations of dispersion equations. These investigations show that transformation of guided waves is determined by analytical properties of dispersion equations in the vicinity of some critical and singular points such as fold points, Morse points, and branch points. Relevant references can be found in [15] and [16]. Extension of such analytical techniques for real absorbing and dispersive materials is very attractive but it seems to be difficult.

ACKNOWLEDGMENT

The authors would like to thank Prof. D. R. Jackson, A. A Oliner, and A. D. Shatrov for discussions on some topics related to the subject of this paper. They would also like to thank the reviewers for their valuable comments as well.

REFERENCES

[1] R. T. Ling, J. D. Scholler, and P. Ya. Ufimtsev, "The excitation and propagation of surface waves in an absorbing layer," in *URSI North Amer. Radio Sci. Meet. Dig.* Montreal, Canada, July 1997, p. 200.

[2] ——, "Transformation of surface waves in absorbing layers," in *USNC/URSI Nat. Radio Sci. Meet. Dig.* Atlanta, GA, June 1998, p. 277.

[3] P. Ya. Ufimtsev and R. T. Ling, "Keynote address: Surface waves in absorbing layers," in *Proc. JINA Int. Conf. Antennas*, Nice, France, Nov. 1998, pp. 3–12.

[4] ——, "Properties of TE surface waves in absorbing layers," in *USNC/URSI Nat. Radio Sci. Meet. Dig.* Orlando, FL, July 1999, p. 35.

[5] R. T. Ling, J. D. Scholler, and P. Y. Ufimtsev, "The propagation and excitation of surface waves in an absorbing layer," *J. Electromagn. Waves Applicat.*, vol. 12, pp. 883–884, 1998.

[6] ——, "The propagation and exitation of surface waves in an absorbing layer," *Progress Electromagn. Res. PIER*, vol. 19, pp. 49–91, 1998.

[7] ——, "Errata to the paper The propagation and excitation of surface waves in an absorbing layer," *PIER*, vol. 19, pp. 49–91, 1998 . *J. Electromagn. Waves Applicat.*, vol. 12, p. 1537, 1998.

[8] J. A. Stratton, *Electromagnetic Theory*. New York: McGraw-Hill, 1941.

[9] H. M. Barlow and J. Brown, *Radio Surface Waves*. London, U.K.: Oxford Univ. Press, 1962.

[10] T. Tamir and A. A. Oliner, "Guided complex waves—Part I: Fields at an interface," *Proc. Inst. Elect. Eng.*, vol. 110, pp. 310–324, 1963.

[11] ——, "The influence of complex waves on the radiation field of slot-excited plasma layer," *IRE Trans. Antennas Propagat.*, vol. AP-10, pp. 55–65, Jan. 1962.

[12] V. V. Schevchenko, "Graphic classification of waves guided by regular open waveguides," *Radio Eng. Electron. Phys.*, vol. 14, no. 10, pp. 1530–1533, 1969.

[13] D. R. Jackson and A. A. Oliner, "A leaky wave analysis of the high-gain printed antennas configuration," *IEEE Trans. Antennas Propagat.*, vol. 36, pp. 905–910, July 1988.

[14] W. H. Press *et al.*, *Numerical Recipes in FORTRAN*. Cambridge, U.K.: Cambridge Univ. Press, 1992, p. 364.

[15] G. W. Hanson and A. B. Yakovlev, "An analysis of leaky-wave dispersion phenomena in the vicinity of cutoff using complex frequency plane singularities," *Radio Sci.*, vol. 33, no. 4, pp. 803–819, July/Aug. 1998.

[16] A. B. Yakovlev and G. W. Hanson, "Mode transformation and mode continuation regimes on waveguiding structures," IEEE Trans. Microwave Theory Tech., to be published.

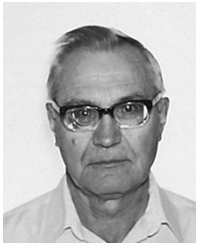

Pyotr Y. Ufimtsev (SM'92–F'99) received the M.S. degree in theoretical physics from the Odessa St. University, Ukraine, in 1954, the Ph.D. degree in electrical engineering from the Central Research Radio Engineering Institute of the Radio Industry, Moscow, Russia, in 1959, and the D.Sc. degree in theoretical and mathematical physics from the St. Petersburg University, St. Petersburg, Russia, in 1970, , and the Professor Scientific degree from the Moscow Aviation Institute, Russia, in 1987.

In 1990, he was a Head Scientist at the Institute of Radio Engineering and Electronics of the USSR Academy of Sciences, Moscow, Russia. In 1990 he was invited to join the University of California at Los Angeles (UCLA). Currently, he is an Adjunct Professor at UCLA and a Principal Engineer at Northrop Grumman Corporation, Pico Rivera, CA. He is the founder of the Physical Theory of Diffraction which is widely used in antennas design and radar-cross-section calculation. In particular, this theory was used in the design of American stealth aircraft and ships.

Dr. Ufimtsev received, for his scientific achievements, the USSR State Prize (Moscow, 1990), the Leroy Randle Grumman Medal (New York, 1991), the 20th Century Award for Achievement Medal and the Hall of Fame Medal (Cambridge, U.K., 1996). He is listed in the Marquis editions *Who's Who in Engineering and Science*, *Who's Who in America*, and *Who's Who in the World*. He was a member of the A.S. Popov Scientific and Technical Society (USSR, 1954–1990) and a member of the Scientific Board on the Problems of Radio Waves Propagation in the Academy of Sciences (USSR, 1960–1990). Currently, he is a member of the United States Electromagnetics Academy (Massachusetts Institute of Technology, Cambridge, MA) and an Associate Fellow of the American Institute of Aeronautics and Astronautics.

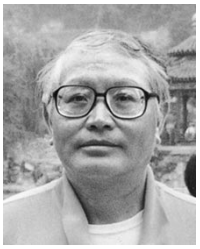

R. T. Ling received the Ph.D. in physics from the University of California, San Diego, in 1972.

He continued his research on quantum scattering theory at the California Institute of Technology, Pasadena, as a Research Fellow. Until 1998 he was involved with computational physics problems related to aircraft design at Northrop Grumman Corporation, Pico Rivera, CA. Currently, he is with the Technical University at Hamburg, Germany.

Dr. Ling is a member of the American Physical Society.

J. D. Scholler (M'84) received his Ph.D. degree in physics from the University of California, Los Angeles, in 1982.

He has worked for a number of aerospace companies in electromagnetics over the past 20 years. His interests have been in the development of numerical techniques for electromagnetic analysis, as well as the design and integration of electromagnetic performance. He is currently working at Northrop Grumman Corporation where he has been developing specifications for the electromagnetic properties of materials produced in the manufacturing environment.